PERFORMANCE OF THE SEASONDE HIGH-FREQUENCY RADAR SYSTEM FOR SURFACE CURRENT MEASUREMENTS

by

Donald O. Hodgins and John S. Hardy

Seaconsult Marine Research Ltd.
8805 Osler Street
Vancouver, B.C. V6P 4G1

ABSTRACT

Intercomparison of currents measured with the new SeaSonde with drifter data have shown the SeaSonde speeds to be unbiased with scatter characterized by a standard deviation of 10.3 cm/s. Mean absolute speed differences averaged 7.8 $\pm$ 6.7 cm/s not accounting for speed errors in the drifters of $\pm$ 4 cm/s. Trajectories calculated from the SeaSonde surface currents showed good agreement with the drifters, reproducing tidally induced loops and eddies in the flow. Separation scales of the predicted and measured trajectories were typically 7 $\pm$ 1.5 km after 36 h and 9 $\pm$ 2 km after 48 h. The SeaSonde currents were judged reliable using the drifters as ground truth, noting the differences in time averaging (none for the drifters and 1 h for SeaSonde) and the depth of flow sensed by each.

1.0 INTRODUCTION

In August of 1991, the new SeaSonde HF radar system (Hodgins, 1991) was deployed at the southern end of the Queen Charlotte Islands to monitor the strong tidal surface currents in that area over a 21-day period. This was the first wilderness deployment of the new system. Four days of near-surface drogued drifter data were also collected for comparison with the radar-measured currents. Some features of the deployment are discussed in this paper, together with the results of the intercomparison, using both Eulerian and Lagrangian methods.

Five Sea Rover drifting buoys were deployed in or near the radar coverage area between August 21 and 24, 1991. Each drifter was fitted with a 5-m long holey sock drogue and eight independent drift tracks were measured, ranging in duration from 17.5 to 48 h (Table 1). The time between position fixes was 30 minutes. The Sea Rover buoys use Loran C for positioning, which in Queen Charlotte Sound is believed to be accurate to no better than $\pm$50 m (pers. comm., W. Crawford, Institute of Ocean Sciences, 1992). The corresponding error in the velocity components is $\pm$4 cm/s.

Winds during this period were moderate, at 10 to 20 knots steady from the northwest, with brief periods of speeds of 5 to 10 knots.

Table 1: Sea Rover Drifter Deployment Times in Queen Charlotte Sound

Drogue Number	Start Date Time (dd/mm/yy) (GMT)	End Date Time (dd/mm/yy) GMT	Length (hours)
G30	21/08/91 17:00	22/08/91 22:00	29.0
H30	23/08/91 07:30	24/08/91 01:00	17.5
E31	21/08/91 18:30	23/08/91 18:30	48.0
H32	21/08/91 20:00	23/08/91 00:00	28.0
I32	23/08/91 07:00	24/08/91 02:00	19.0
I37	22/08/91 17:30	24/08/91 03:00	33.5
G38	21/08/91 20:30	23/08/91 01:30	29.0
H38	23/08/91 05:30	24/08/91 04:30	23.0

2.0 DEPLOYMENT AND MEASUREMENT PROPERTIES

The rugged, inaccessible terrain on the east coast of Khunghit Island provided only two possible sites at which to locate the radar units: Cape St. James (the weather station) and Lyman Point (a tiny island), located 16.8 km along the baseline as shown in Fig. 1. This is a comparatively short baseline separation (ideally the radars are separated by about 40 km) resulting in a total current coverage area occupying a small fraction of the dual-radar illumination region defined by the radar measurement range of 60 km.

Portability and low power demand were two of the design objectives for the new radar units. The photographs in Fig. 2 show the installation at Lyman Point. The RF hardware and data acquisition computer was housed in a two-man Hurritent, all powered off a single 2,500 W portable generator. The receive antenna was located about 40 m from the tent, separated from the transmit antenna by roughly 25 m. Both antennas were mounted on standard surveyor's tripods, and required only a small clear area exposed to the ocean. The set-up time for one radar unit was under two hours once the site had been prepared by clearing an area for the tent and generator.

HF radar principles for measuring surface currents are summarized in Hodgins (1991) and Hardy et al. (1989), and are described in detail in Lipa and Barrick (1983). In the new SeaSondes an FMCW (frequency-modulated continuous wave) signal format is used, centered at a frequency of 12.5 MHz. Range resolution is achieved by sweeping the frequency linearly over a 50 kHz band yielding a range resolution of 2.557 km. There are 31 range cells, giving a total theoretical range of just over 79 km. The voltages from each receive antenna are Fourier transformed using a 512-point FFT. The spectral resolution is 0.00390612 Hz, which for the radar frequency of 12.5 MHz is equivalent to a Doppler velocity resolution of approximately 3.3 cm/s. A running spectral average is then formed from 14 consecutive sample spectra, and the averaged Doppler spectra in each range ring were

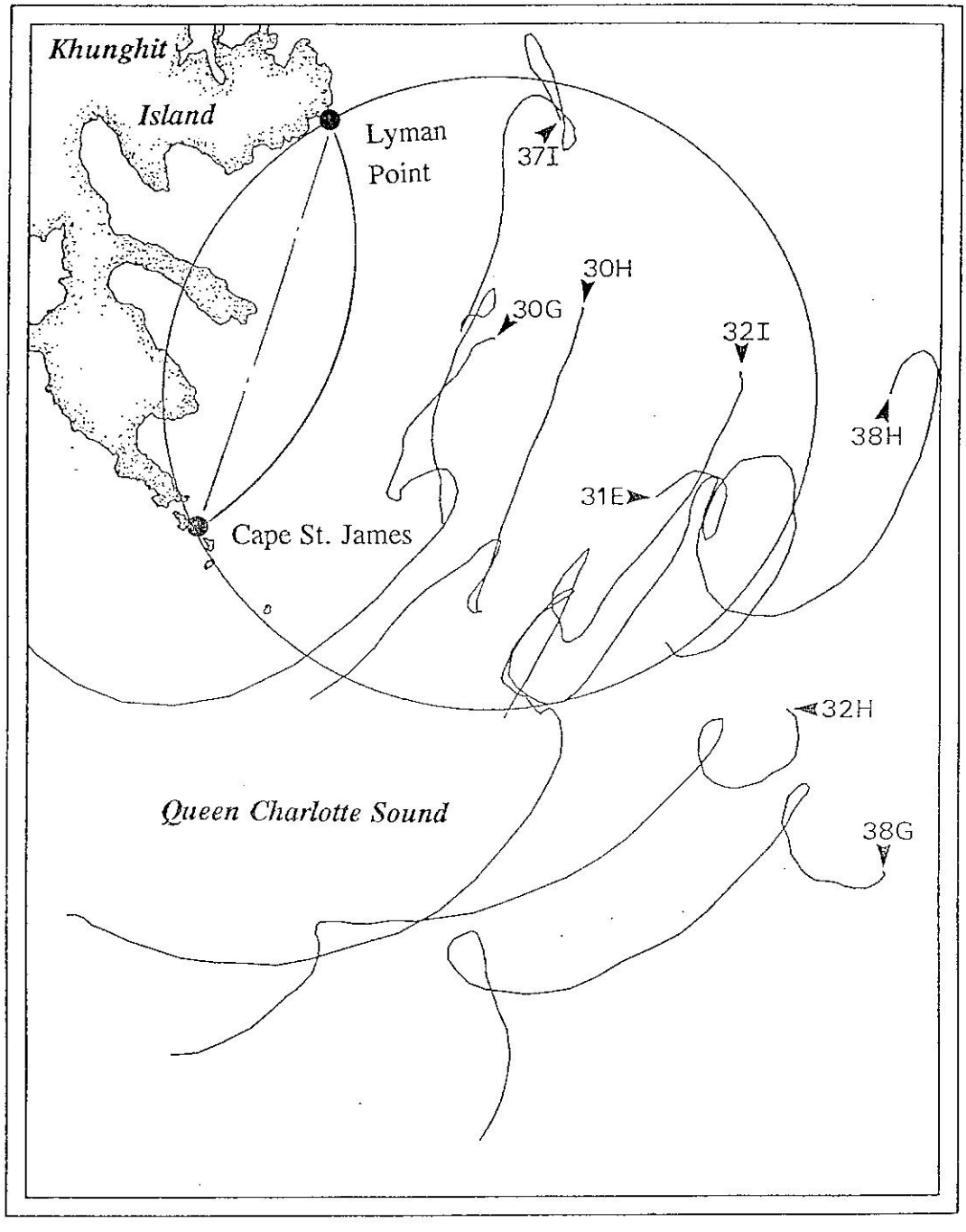

Figure 1 Map of Queen Charlotte Sound and Khunghit Island showing the radar locations and the eight drifter trajectories. The circle describes the two-site coverage area for the baseline joining Cape St. James and Lyman Point.

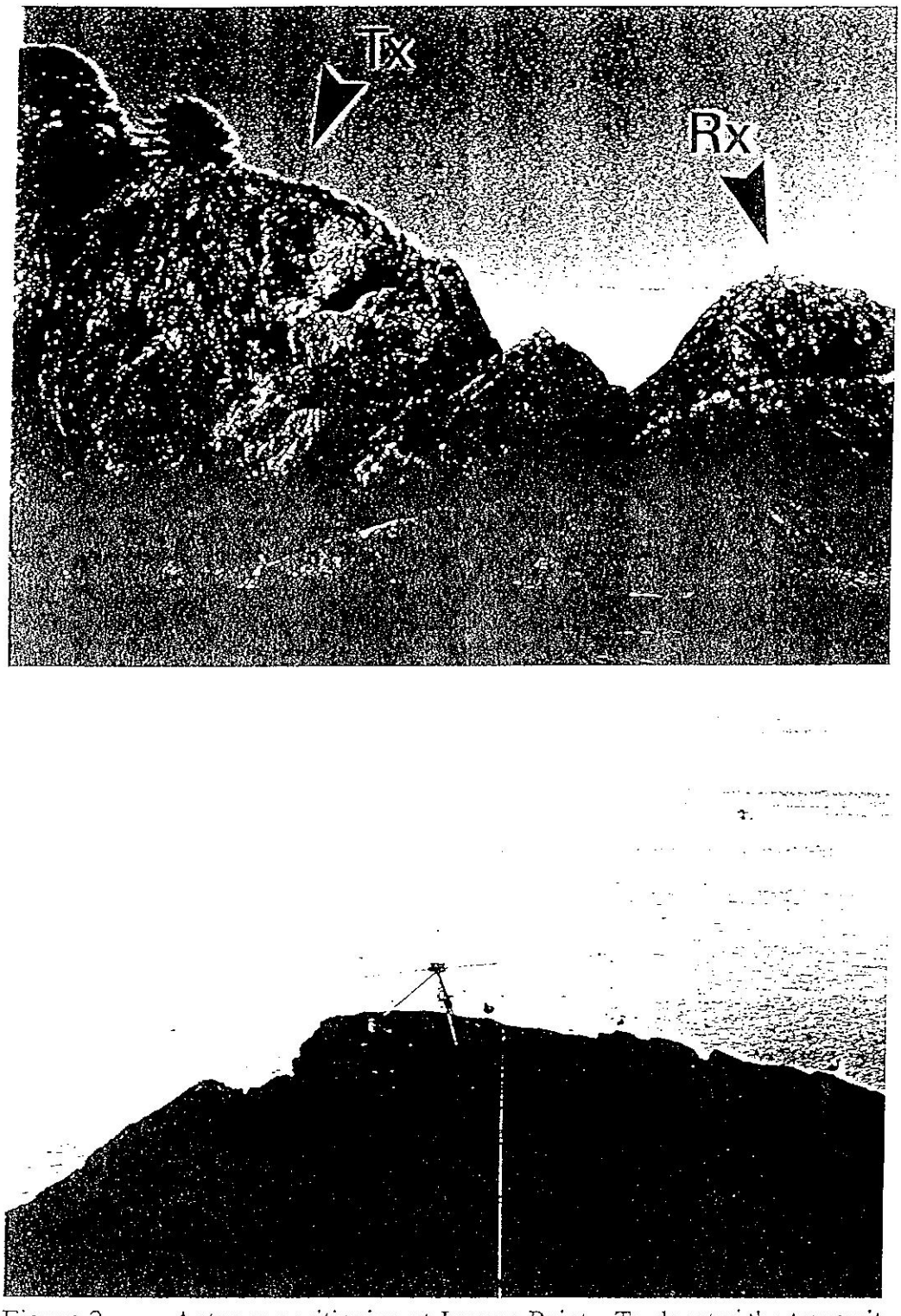

Figure 2 Antenna positioning at Lyman Point. Tx denotes the transmit antenna and Rx denotes the receive antenna. The receive antenna is shown in the lower photograph. All RF hardware and data acquisition computer was housed in a two-man tent in the pine trees above the Tx antenna, powered from a single portable generator.

used for the extraction of radial velocities. Thus, the radial velocities represent a 1-h time average of the actual flow field.

3.0 SURFACE CURRENT CALCULATION

Radial velocities at each radar were extracted from the sea-echo spectra using the least-squares method described by Lipa and Barrick (1983). The method statistically tests the single and dual-angle models for radial currents and selects the one having the best fit to the data. The DF procedure yields the azimuth angles as a function of radial velocity. This function must be inverted to give the radial velocity map, and is done on a regular grid of points in polar coordinates. The azimuthal increment used in the present analysis was 5°. This method of radial current extraction yields optimum estimates of the speed, v, and its standard deviation, δv, at each angle in the field of view.

Total current vectors were calculated by combining the radial data from each radar site on a 1 km by 1 km Cartesian grid (EW-NS orientation) within the coverage area. The coverage area was divided into area cells, and all radial velocities from both radars falling into a given cell were interpreted to give a total current velocity. The circular area cells have been centered on each Cartesian grid point and defined by a blending radius R_b. The total current speed and direction were found by least-squares fitting to the radial components following the algorithm described in Lipa and Barrick (1983). Two thresholds were imposed on each radial velocity, v, in the area cell: $\delta v \leq 10$ cm/s and $v \leq 200$ cm/s. If either threshold was exceeded, that radial velocity was excluded from the fitting procedure. An example of one pair of radial currents maps, and the corresponding total vector field is shown in Fig. 3.

The coverage area is defined by the triangulation angle γ, which is the angle between azimuths from each radar site, intersecting at a combining grid point. Leise (1984) has shown that velocity errors are a function of γ; the minimum error is found at $\gamma = \pi/2$, and increases as γ tends to zero and 180°. Leise presents criteria defining the coverage area as a locus of points satisfying the geometrical error function with $\epsilon = 2$. These criteria have been used to define the coverage area shown in Fig. 1.

4.0 OPTIMUM BLENDING RADIUS

There is no objective criterion for selection of the blending radius R_b. It must be large enough to provide a sufficient number of radial components to define the total vector with confidence, but not so large that it smooths out real features of the current field. By assuming that the drifter data provide a true measure of the surface current, the hypothesis that an optimum blending radius value exists that minimizes the difference in measured current speeds, and hence gives the highest accuracy, was tested. Two statistics have been examined: the difference between SeaSonde and drifter

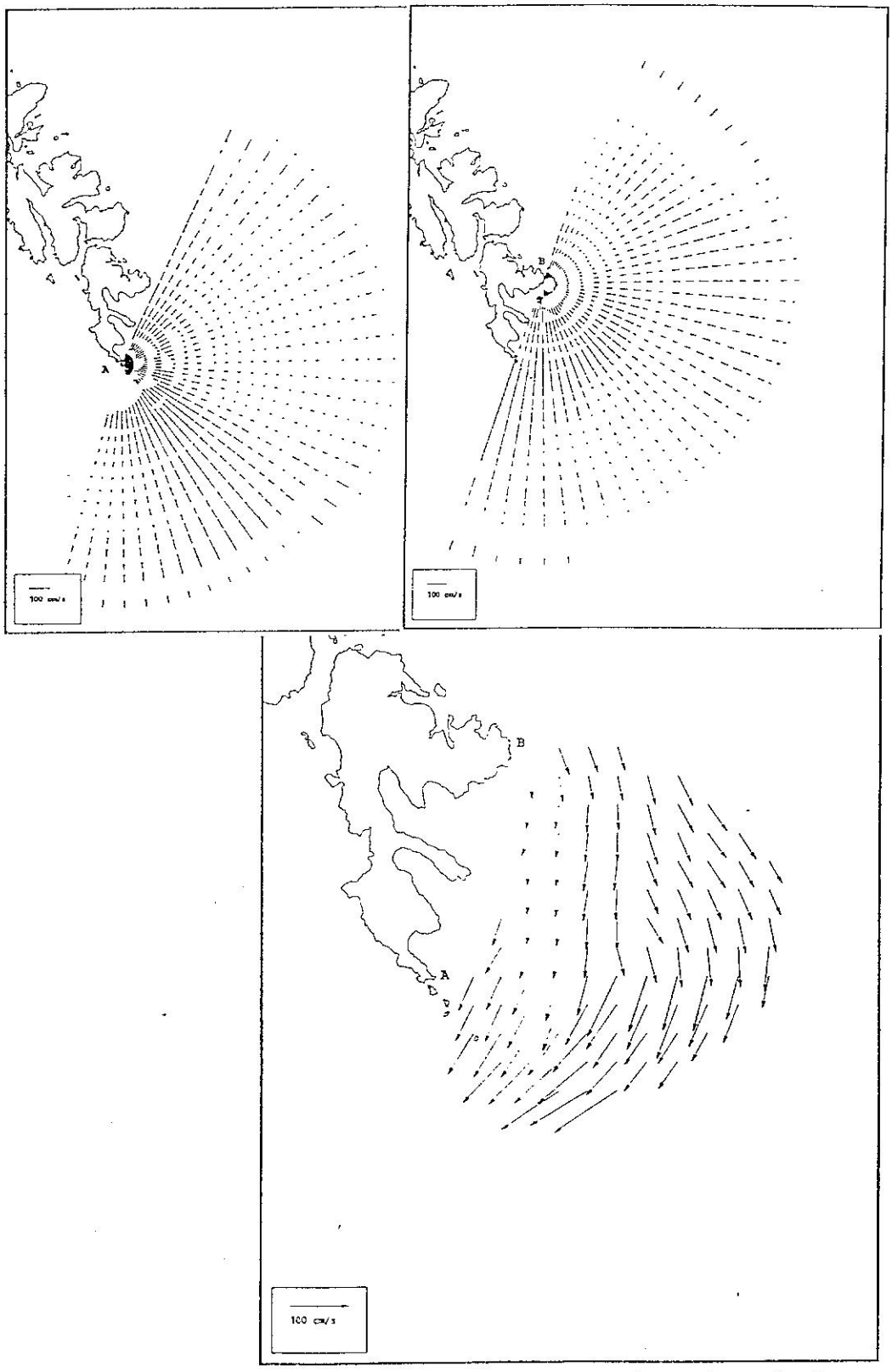

Figure 3 Examples of radial current components from Cape St. James and Lyman Point, and the combined total surface current map.

current speeds (R_s-R_d), which is a measure of bias, and the absolute difference in speed, $|R_s-R_d|$.

The tests were performed using two drifter trajectories centrally located in the coverage area. The mean value of each difference in speed has been calculated for averaging radii varying between 2 and 10 km. The drifter speed R_d has been calculated as the straight-line distance travelled between successive position fixes divided by 30.0 minutes. The SeaSonde speed R_s was calculated as an average along the space-time path defined by the drifter trajectory using the hourly radial current fields for interpolation.

Mean values for 104 observations of (R_s-R_d) and $|R_s-R_d|$ are shown in Fig. 4. The variation of $|R_s-R_d|$ exhibits distinct minimum at radii of 4.5 to 5.5 km, while the bias error has a zero-crossing at about 5.3 km. The bias has a second zero-crossing at 3.25 km; however, the coincidence of zero bias and a minimum in the absolute difference at about 5 km suggests that this is the optimum radius for blending the radial data.

4.0 COMPARISON OF SEASONDE AND DRIFTER CURRENTS

4.1 Eulerian Statistics

Radial Current Components. Radial current speeds (components oriented towards or away from each radar) are compared with the equivalent drifter component speeds for three trajectories (I37, H30, and H38) in Fig. 5. Two of the trajectories are centered in the coverage area, and one (H38) lies mainly outside the area. The radial current at each drifter position has been calculated from the SeaSonde data using a 4-point bilinear interpolation in range and bearing, weighted inversely by the variance of each radial speed. If one or more of the radials were missing, the comparison point was omitted. Generally, the data from each site plot on opposite sides of zero. The correlation of radial speeds is high for all drifters; however, the scatter is slightly greater at H38 than at closer ranges.

Surface Current Vectors. Surface currents components, combined with a radius R_b = 5 km, are compared with the drifter current vectors for tracks I37 and H30 in Fig. 6. These tracks were chosen for their central position in the coverage area. Speeds ranged from less than 5 cm/s to over 80 cm/s, and the SeaSonde shows a high correlation with the drifter data.

The average absolute difference in total current speed for these trajectories (104 observations) is 7.8 cm/s with a standard deviation of 6.7 cm/s. Assuming that about $\pm$4 cm/s of this difference is accounted for by the error in the drifter velocity, it appears that the radar and drifter differ by about an equivalent amount. The drifter speeds are calculated from punctual data, and thus do not provide an equivalent measure to the 1-h average of the SeaSonde. Moreover, the drifters integrate about 5 m of the surface shear, and differ slightly from the SeaSonde measurement. Thus, the additional

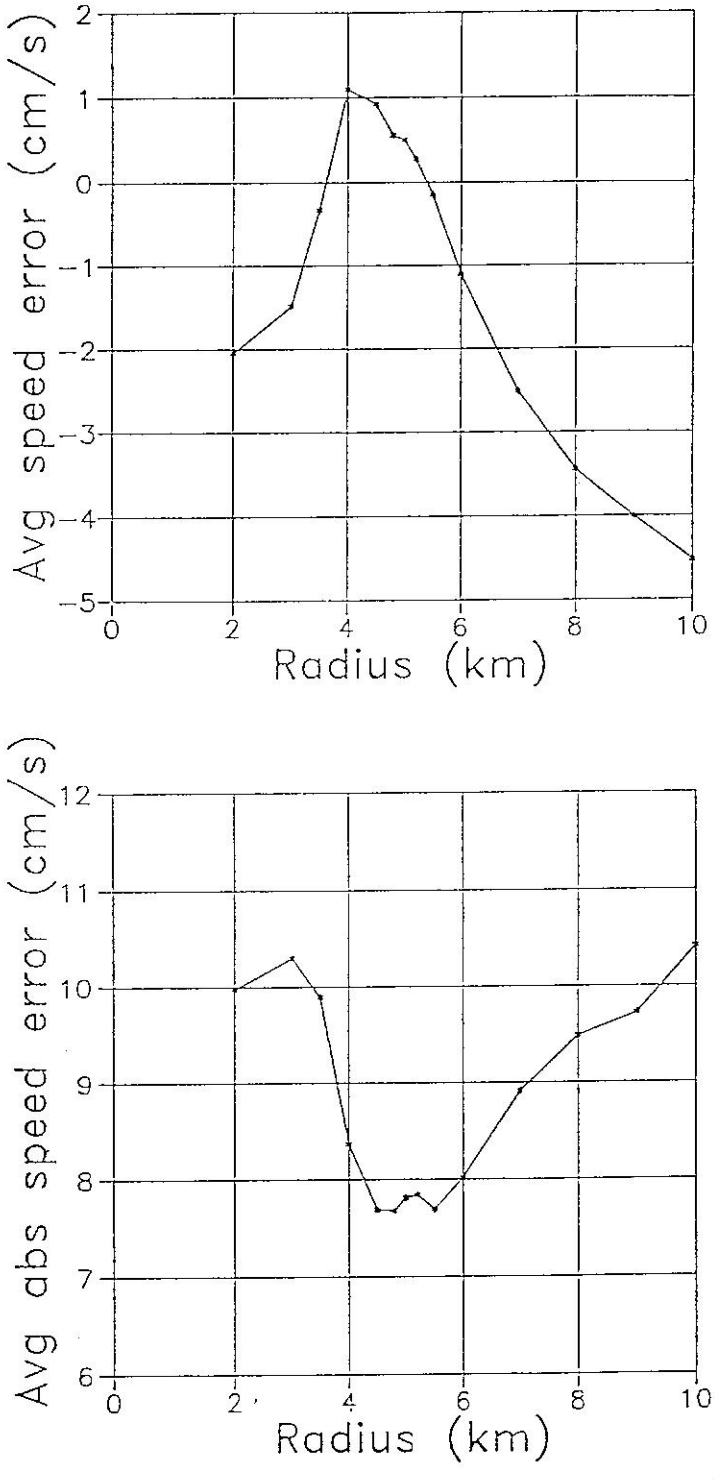

Figure 4 Average speed error (upper panel) and average absolute speed error (lower panel) versus blending raidus R_b for drifters H30 and I37.

difference of ±3 to ±4 cm/s likely arises from the real difference between the surface current and the 5-m drogued drift current, and from error in the radar measurement.

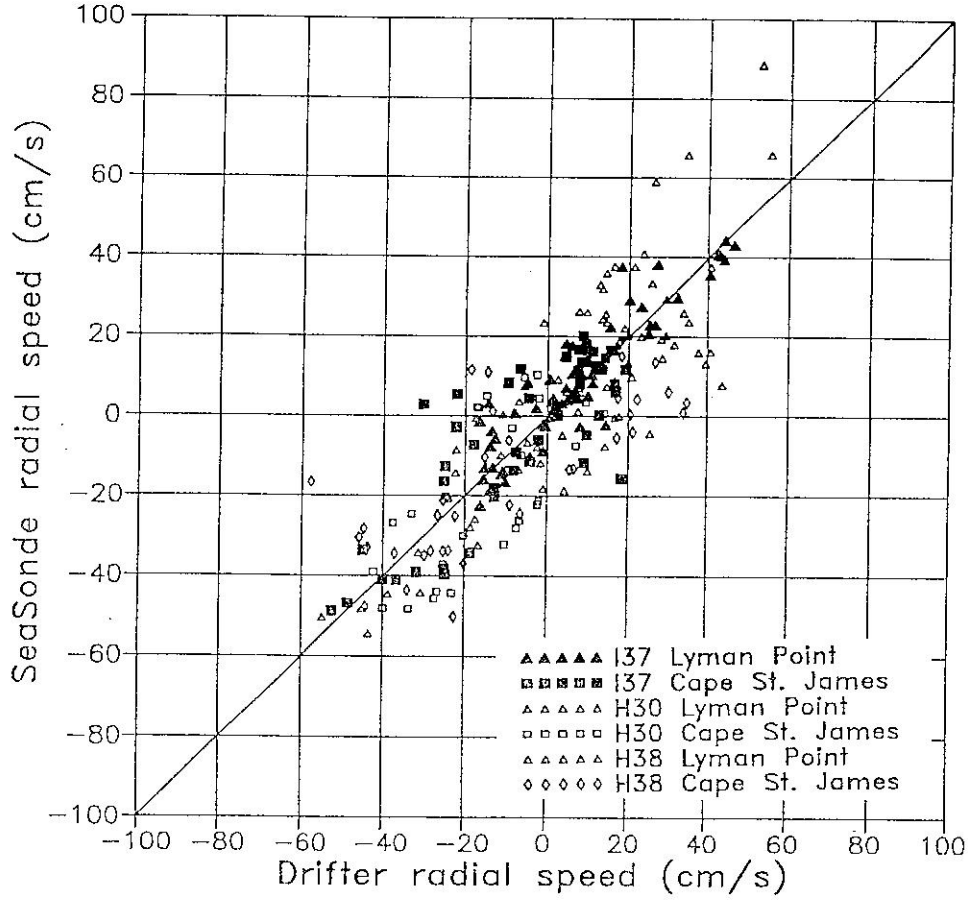

Fig. 5 Scatter diagram of SeaSonde versus drifter radial current speed.

4.2 Lagrangian Comparison

The currents measured with the radar have been used to calculate a set of trajectories initialized at the time and location of the beginning of the measured drift tracks. The predicted trajectories have been calculated from the relation

$$\mathbf{X}(t) = \int_0^t \mathbf{U}_s(\mathbf{x},t)\, dt \qquad (4.1)$$

where $\mathbf{X}$ is the position vector and $\mathbf{U}_s$ is the surface current vector derived from the SeaSonde radial currents with R_b = 5 km. The integral in (4.1) was solved in a sequence of N discrete time steps with increment Δt such that N evenly divided the 30-minute time step of the drifter positions. N was varied between 1 (Δt=30 min) to 15 (Δt=2 min) and the separation distances were compared to determine if the predicted tracks were sensitive

to the integration time step. Predicted drift positions were calculated every 30 minutes, corresponding with the measured trajectories.

A two-step predictor-corrector procedure (indicated in the following equation by subscript l), applied at each integration subinterval Δt, was used to integrate (4.1) for each 30 min time increment, i.e.

$$\mathbf{X}(N\Delta t) = \sum_{n=0}^{N} <_l \mathbf{U}_s> \cdot \Delta t + \mathbf{X}(0\Delta t), \quad l=1,2 \qquad (4.2)$$

where $<_l \mathbf{U}_s> = (\mathbf{U}^{n+1} + \mathbf{U}^n)/2$, with $\mathbf{U}^{n+1} = \mathbf{U}^n$ for $l=1$.

Mean separation distances, defined by $(\mathbf{X}_s - \mathbf{X}_d)$, and standard deviations, were calculated for four trajectories to test the sensitivity of position to the value for N. It was found (see Hodgins and Hardy, 1992) that no increase in accuracy was achieved with a space-time step of integration less than 30 min.

Representative comparisons of predicted and measured trajectories are shown in Fig. 6 and 7. The trajectories generally exhibit good agreement, where many of the tidally induced eddy-like features found in the drifter tracks are reproduced by the SeaSonde predictions. On balance, the total displacement of the SeaSonde tracks is slightly greater than the drifters, consistent with a stronger currents right at the sea surface than integrated over the drogue depth.

Separation $(\mathbf{X}_s - \mathbf{X}_d)$ versus elapsed time is plotted in Fig. 8 for each of the six drift tracks. The longest trajectory, I37, was modelled well, with the separation distance increasing more-or-less steadily with time. After 33 h the separation was about 7 km. Except for drifter H38, the separation distance generally increased with time and was bounded above by 7 km about 15 to 20 h after release.

The mean separation and one standard deviation are plotted in Fig. 9 for elapsed times out to 15 h. This is the longest time for which meaningful averages could be obtained. These results show that the separation distance tends to increase steadily for about 6 h, after which it assumes a roughly constant value of about 3 to 4 km. This tendency to a constant separation was consistent with the observed behaviour of the tracks, four of which tended to converge between 5 and 15 h, while two others continue to diverge, with some small variations. The average works out to a roughly constant value.

5.0 CONCLUSIONS

The combining radius for processing radial current components from two radar units has been shown to have an optimum value within the centre of

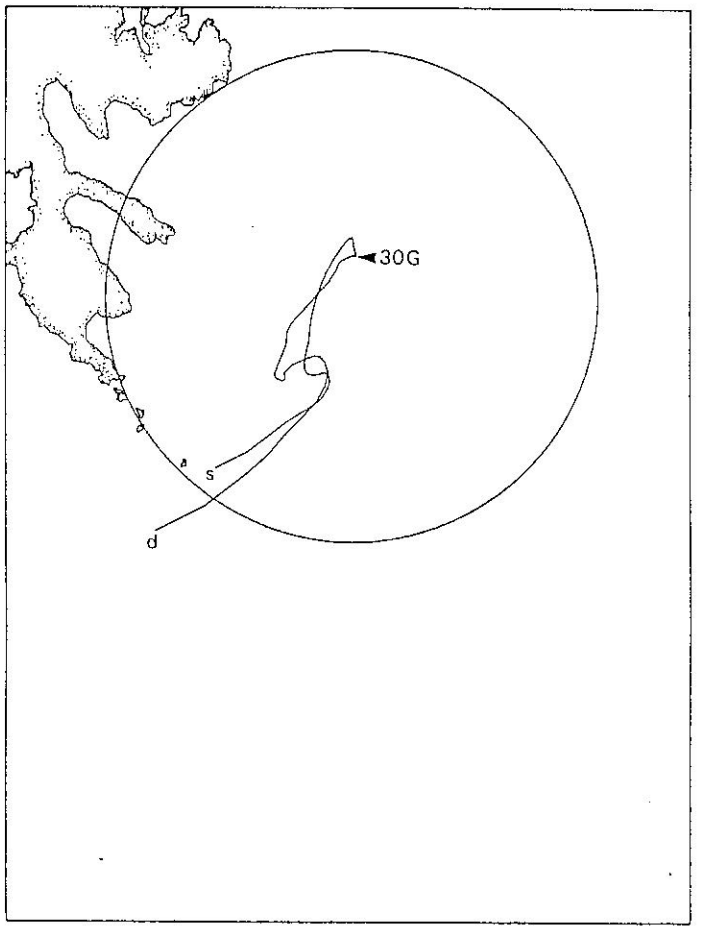

Figure 7 Comparison of predicted (s) and measured (d) drift track for trajectory G30.

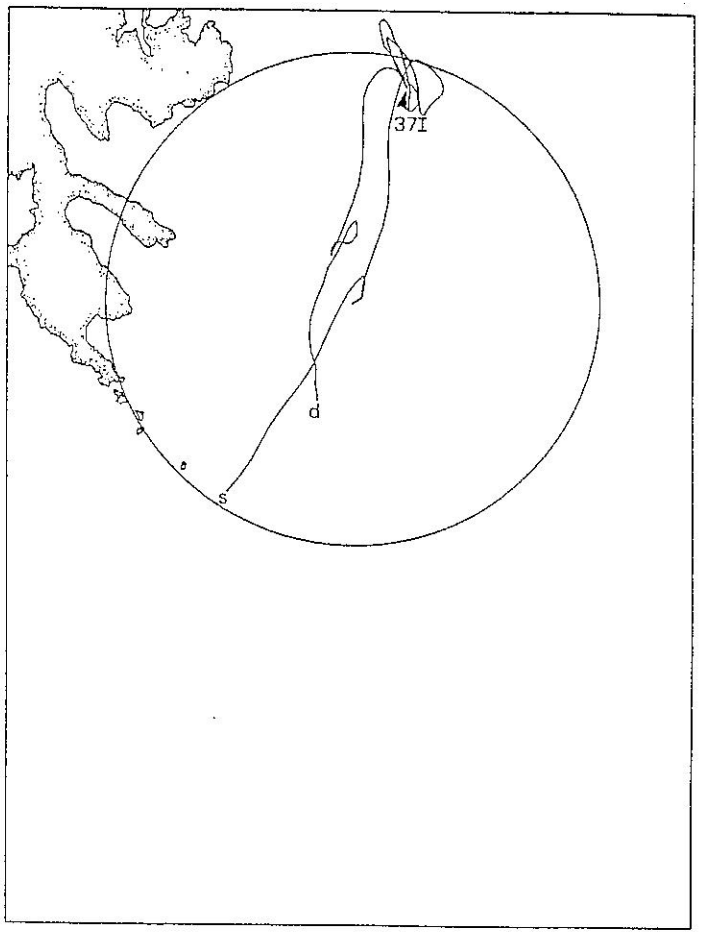

Figure 6 Comparison of predicted (s) and measured (d) drift track for trajectory I37.

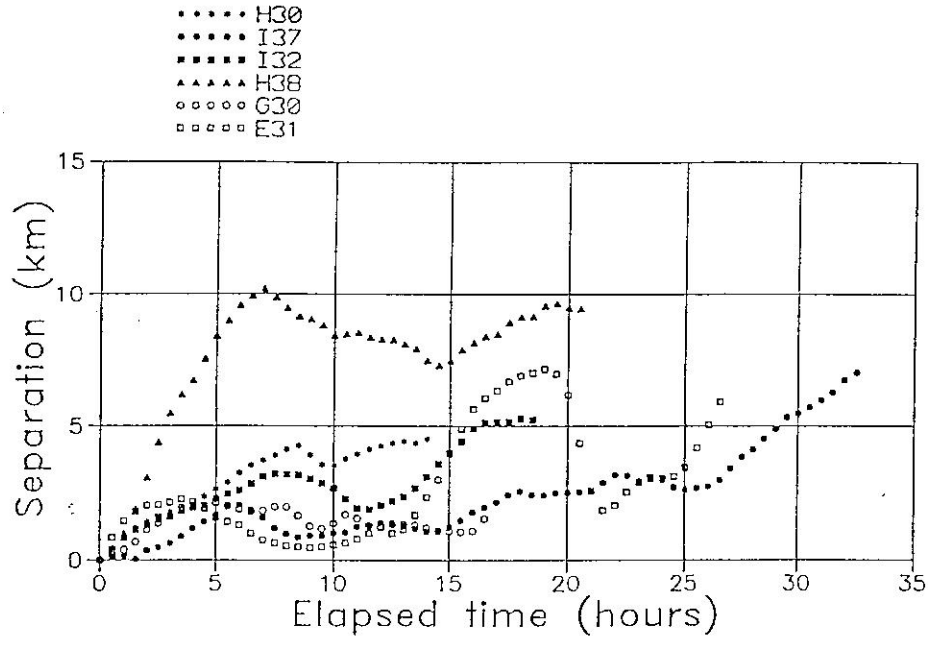

Figure 8 Separation distance versus drift time.

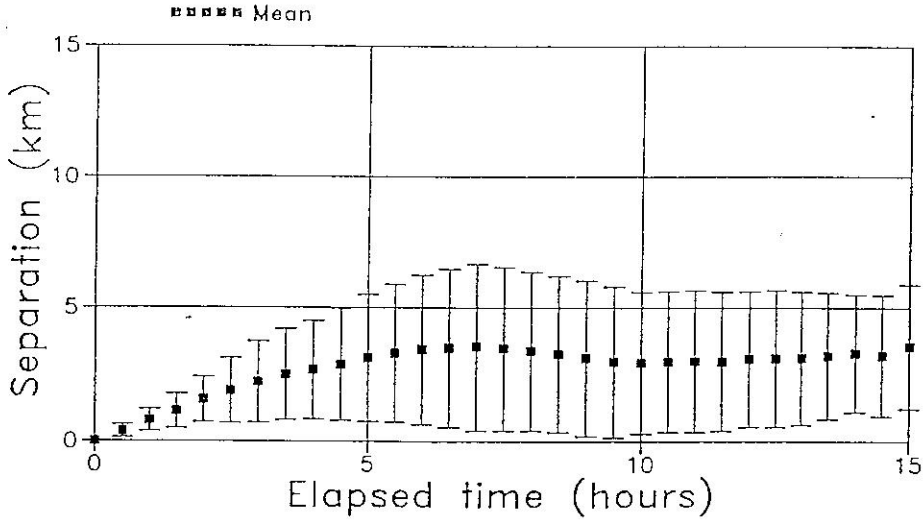

Figure 9 Average separation distance versus elapsed drift time.

the coverage area. Using the drifters to provide ground-truth data, the optimum radius for the Queen Charlotte Island deployment was 5 ± 0.5 km. Comparison of both radial and combined total current speeds and directions with individual drifter tracks showed a high correlation. In the coverage area the mean absolute difference between drifter currents and SeaSonde currents was about 7.8 cm/s with a standard deviation of 6.7 cm/s for currents ranging up to 80 cm/s. The results were essentially unbiased (mean difference of 0.25 cm/s and standard deviations of 10.3 cm/s). The drifter speed error is estimated to be about ±4 cm/s based on the positional uncertainty of Loran-C in the study area.

A Lagrangian comparison showed that predicted drift from the SeaSonde data reproduced the tidally-induced eddies and loops exhibited by the drifters, as well as the overall drift patterns. The drifters were deployed for periods of 17 to 48 h. Characteristic separation distances in these times were about 5 to 7 km. The worst case from a drifter slightly outside the coverage area showed separations of 10 km within 7 h of release.

Based on linear regression of the separation distance with time for the three longest tracks, representative separation scales are 7 ± 1.5 and 9 ± 2 km for drift times of 36 and 48 h for targets within the coverage area of the radars. If the drifters are assumed to represent true positions, predicted drift with errors of this magnitude provide suitably accurate results for oilspill modelling. However, the drifters measure currents that are different from the SeaSonde, and some of the separation results from the differences in the currents as measured in each manner. Consequently, SeaSonde drift predictions for surface-floating objects may be more accurate than suggested by the drifter comparison. In order to better quantify the accuracy of SeaSonde predicted trajectories, a near-surface drifter with an effective penetration into the water of less than 2 m is required.

6.0 ACKNOWLEDGEMENTS

The deployment of the SeaSonde radar system, and collection of the drifter data for comparison with the surface current measurements, was undertaken as part of PERD Project 62142, administered by Fisheries & Oceans Canada (Dr. D. Masson). Funding was also provided by the Emergencies Science Division of Environment Canada and the Canadian Coast Guard.

7.0 REFERENCES

Hardy, J.S., D.S. Dunbar and D.O. Hodgins, 1989. An Evaluation of Methods for Extracting Surface Currents from CODAR Data. Proc. IGARRS '89, 12th Canadian Symposium on Remote Sensing, Vancouver, Canada.

Hodgins, D.O., 1991. New Capabilities in Real-time Oil Spill and Fate Prediction Using HF Radar Remote Sensing. Proc. 14th AMOP Technical Seminar, June 12-14, 1991, Vancouver, Canada.

Hodgins, D.O. and J.S. Hardy, 1992. Surface Current Data from Queen Charlotte Sound, B.C., Intercomparison of SeaSonde and Drifter Current Observations. Prepared for Fisheries & Oceans, Canada, Canadian Coast Guard, and Environment Canada by Seaconsult Marine Research Ltd.

Leise, J.A., 1984. The analysis and digital signal processing of NOAA's surface current mapping system," *IEEE J. Ocean. Eng.*, **OE-9**(2), 106-113.

Lipa, B.J. and D.E. Barrick, 1983. Least-Squares Methods for the Extraction of Surface Currents From CODAR Crossed-Loop Data: Application at ARSLOE. IEEE *J. Oceanic Eng.*, OE-8(4), 226-253.

PROCEEDINGS OF THE FIFTEENTH ARCTIC AND MARINE OIL SPILL PROGRAM TECHNICAL SEMINAR

COMPTE RENDU: 15e COLLOQUE TECHNIQUE DU PROGRAMME DE LUTTE CONTRES LES DÉVERSEMENTS D'HYDROCARBURES EN MER ET DANS L'ARCTIQUE (AMOP)

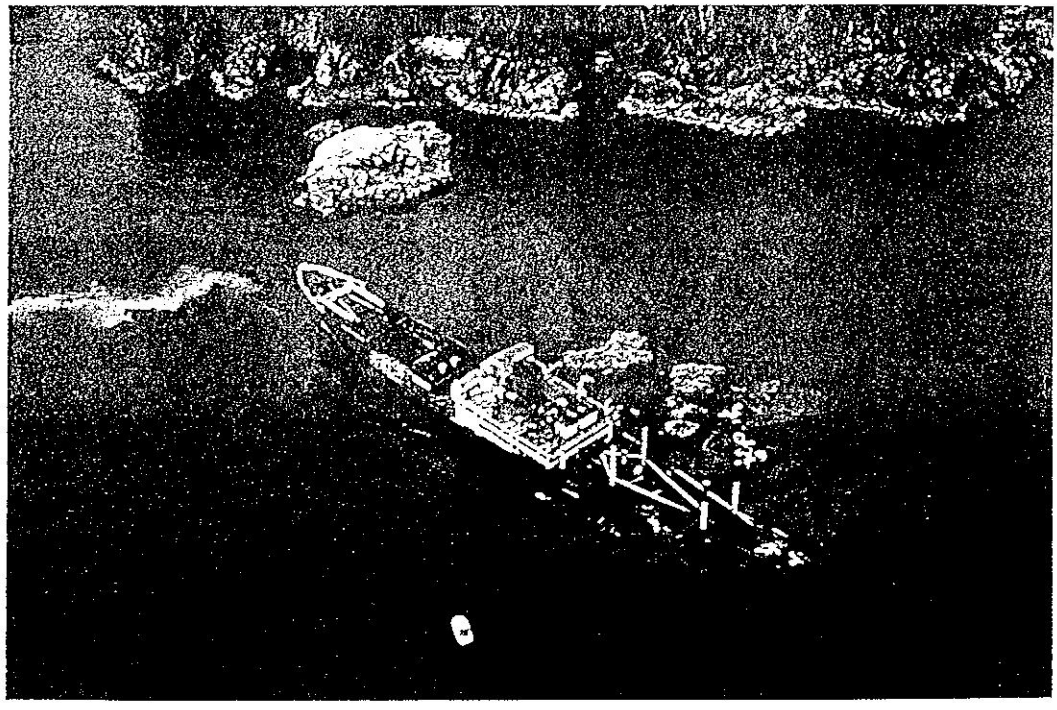

JUNE 10-12, 1992
EDMONTON, ALBERTA

DU 10 AU 12 JUIN, 1992
EDMONTON (ALBERTA)

Environment Canada Environnement Canada

Canada